Nuclear diagnostics for the National Ignition Facility (invited)

Thomas J. Murphy,[a)] Cris W. Barnes, R. R. Berggren, P. Bradley, S. E. Caldwell,
R. E. Chrien, J. R. Faulkner, P. L. Gobby, N. Hoffman, J. L. Jimerson, K. A. Klare,
C. L. Lee, J. M. Mack, G. L. Morgan, J. A. Oertel, F. J. Swenson, P. J. Walsh,
R. B. Walton, R. G. Watt, M. D. Wilke, D. C. Wilson, and C. S. Young
Los Alamos National Laboratory, Los Alamos, New Mexico 87545

S. W. Haan, R. A. Lerche, M. J. Moran, T. W. Phillips, and T. C. Sangster
Lawrence Livermore National Laboratory, 7000 East Avenue, Livermore, California 94550

R. J. Leeper and C. L. Ruiz
Sandia National Laboratories, Albuquerque, New Mexico 87185

G. W. Cooper
University of New Mexico, Albuquerque, New Mexico 87131

L. Disdier, A. Rouyer, and A. Fedotoff
Commissariat à l'Energie Atomique, Bruyères le Châtel, BP 12, 91680 Bruyères le Châtel, France

V. Yu. Glebov, D. D. Meyerhofer, J. M. Soures, and C. Stöckl
*Laboratory for Laser Energetics, University of Rochester, 250 East River Road, Rochester,
New York 14623-1212*

J. A. Frenje, D. G. Hicks, C. K. Li, R. D. Petrasso, and F. H. Seguin
Massachusetts Institute of Technology, Plasma Fusion Center, Cambridge, Massachusetts 02139-0001

K. Fletcher and S. Padalino
Department of Physics, State University of New York, Geneseo, New York 14454

R. K. Fisher
General Atomics, San Diego, California 92186

The National Ignition Facility (NIF), currently under construction at the Lawrence Livermore National Laboratory, will provide unprecedented opportunities for the use of nuclear diagnostics in inertial confinement fusion experiments. The completed facility will provide 2 MJ of laser energy for driving targets, compared to the approximately 40 kJ that was available on Nova and the approximately 30 kJ available on Omega. Ignited NIF targets are anticipated to produce up to 10^{19} DT neutrons. In addition to a basic set of nuclear diagnostics based on previous experience, these higher NIF yields are expected to allow innovative nuclear diagnostic techniques to be utilized, such as neutron imaging, recoil proton techniques, and gamma-ray-based reaction history measurements. © *2001 American Institute of Physics.* [DOI: 10.1063/1.1319356]

I. INTRODUCTION

The National Ignition Facility[1] (NIF) is a 192 beam laser system (Fig. 1) currently under construction at Lawrence Livermore National Laboratory. When completed, the NIF will be able to deliver 1.8 MJ of laser energy to a target. On its current schedule, the NIF will deliver first light to the target chamber center in late FY 2004 and will be completed in late FY 2008. The first neutron producing experiments would occur near mid-FY 2006.

One of the main missions of the facility is to achieve thermonuclear ignition of fusion fuel using the indirect drive approach of inertial confinement fusion (ICF).[2] In this mission, the laser beams will be used to heat a ''hohlraum,'' producing a uniform x-radiation field which heats the outer surface of a capsule. A typical ICF capsule design has an ablator, a layer of frozen deuterium–tritium (DT) fuel, and DT gas. The pressure of the vaporizing ablator drives the capsule inward, compressing and heating the DT fuel. The convergence of a number of shocks raises the temperature of the DT gas to the point that nuclear fusion begins. If the fuel layer has been compressed to high enough density, the alpha particles deposit their energy in the fuel, raising it to thermonuclear temperatures, and the thermonuclear burn propagates, consuming a large fraction of the fuel.

Nuclear diagnostics can be used to measure many of the properties of this implosion process and include nuclear yield, ion temperature, electron temperature, implosion time, burn width/burn history, burn region, fuel areal density (ρR), ablator areal density ($\rho \Delta R$), and shell mix.

Nuclear diagnostics have been identified, as well, as the indicators of ignition, with a rapid rise in nuclear yield or ion temperature with some progressive change in experimental conditions being seen as a good indicator of alpha particle deposition in the fuel.[2]

a)Electronic mail: tjmurphy@lanl.gov

Nuclear diagnostics have both advantages and disadvantages compared to other diagnostics. Advantages include the highly penetrating nature of neutrons, gamma rays, and high energy protons. This allows diagnosis of the core of an imploded capsule, even with very dense implosions. In addition, the fact that the products of the fusion reactions are being measured makes nuclear diagnostics effective at determining the overall effectiveness of a target design, since creating fusion products is, in fact, the ultimate goal. Disadvantages include the fact that information can be obtained only near the time of peak compression, since this is when fusion products are created. Nuclear diagnostics are, of course, not applicable to the wide range of experiments that have no nuclear yield, such as x-ray drive,[3] planar hydrodynamics,[4] materials properties,[5] or most laser-plasma instability experiments.[6] The subset of fusion products that can escape an imploded capsule must be very penetrating, and therefore they are very difficult to image.

The utility of nuclear diagnostics for ICF and other high energy density physics experiments has been demonstrated, and a wide range of nuclear diagnostics is being developed and designed for the NIF. The requirements are broader than has been required on previous ICF facilities. Neutron yields will need to be measured over roughly 13 orders of magnitude, from the lowest yields of about 10^6 DD neutrons, up to high gain implosions yielding 10^{19} DT neutrons, or about 30 MJ of fusion energy. Ion temperatures will need to be measured from 1 up to 50 keV for targets yielding more than about 3×10^7 neutrons. The average emission time of neutrons needs to be established with 100 ps accuracy for laser pulse lengths up to 20 ns long.

II. CORE NUCLEAR DIAGNOSTICS

A set of ''core'' diagnostics has been identified. A diagnostic is considered core if it is required to measure the interaction of the laser beams with the targets, has a wide user base and strong programmatic requirements, and requires minimal R&D.[7] Thus, the core diagnostics are known techniques that have been successfully utilized on previous large lasers and are known to work. Table I lists the core nuclear diagnostics along with the institution responsible for each.

A. Activation measurements

The total neutron yield from ICF targets will be determined by an absolutely calibrated neutron activation system.[8,9] An activation sample, consisting of a suitable material, will be placed at some known distance from the ICF target and irradiated with the neutrons produced in the experiment. The neutrons will render the sample radioactive by an amount proportional to the neutron fluence experienced by the sample. The activated sample will then be removed from the target area to have its radioactivity measured and the yield from the experiment determined.

The yield from the target Y_n produces a number of counts in the detector N_γ given by

$$N_{\gamma,\infty} = \frac{Y_n}{4\pi r^2} \frac{m N_A a \sigma f}{A} \epsilon \eta_{sa} \eta_{\text{trans}}, \tag{1}$$
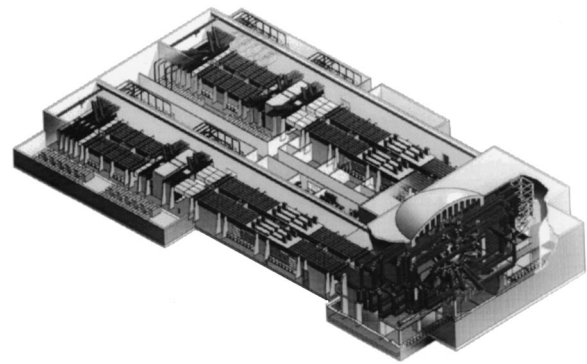

FIG. 1. The National Ignition Facility is a 192 beam, 2 MJ glass laser currently under construction at Lawrence Livermore National Laboratory.

where $N_{\gamma,\infty}$ is the number of gamma counts that would have been measured had counting begun immediately after the implosion and continued indefinitely, Y_n is the neutron yield, r is the distance from the neutron source to the activation sample, m is the mass of the sample, N_A is Avagadro's number, f is the branching ratio of the decay, A is the atomic mass of the activation sample, a is the abundance of the isotope being activated, ϵ is the efficiency of the counting system, η_{sa} is a factor which accounts for self-absorption of the gamma radiation in the sample, and η_{trans} accounts for neutron scattering in the sample itself. The actual counts N_γ are related by the expression

$$N_\gamma = N_{\gamma,\infty} e^{-\tau_{\text{delay}}/\tau}(1 - e^{-\tau_{\text{count}}/\tau}), \tag{2}$$

where τ is the decay time for the decay, τ_{delay} is the time between the implosion and the start of counting, and τ_{count} is the duration of the counting.

The method of operation and calibration will be determined by the neutron yield to be measured. For relatively low yield (below about 10^{14} DT neutrons), the system will consist of samples with mass on the order of tens of grams. The transport of neutrons in the sample, as well as the self-absorption of the radiation emitted by the sample, may be significant. In addition, the counting geometry is designed to be very efficient, but makes absolute calibration of the detector difficult. However, the method of calibration removes these issues. The sample is exposed to a known neutron fluence from a neutron generator in which the neutron production is monitored by measuring the ''associated particle'' in the reaction in which the neutron is produced.[10] For the DT reaction, the alpha particle created in the reaction is monitored, and a fluence at the activation sample is determined. With this method of calibration, Eq. (1) reduces to

TABLE I. Nuclear diagnostics which constitute a subset of the NIF ''core'' diagnostics and the institutions responsible for providing those diagnostics.

| Diagnostic system	Institution responsible
Activation system/low yield	Sandia National Laboratories
Activation system/high yield	Los Alamos National Laboratory
Neutron time of flight	Los Alamos National Laboratory
Neutron emission time	Los Alamos National Laboratory
Neutron spectrometer	Los Alamos National Laboratory
Debris/radiochemistry	Nuclear Weapons Effects program
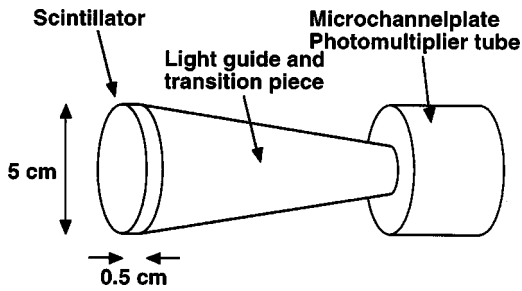
FIG. 2. Schematic of a typical current-mode neutron detector. The dimensions listed are for nToF-6 and nToF-17.

TABLE II. Specifications for each of the detectors in the neutron time of flight (n ToF) and emission time (ET) system for the NIF.

Detector	Diameter (cm)	Thickness (cm)	Distance (m)	Main purpose
n ToF-ET (emission time)	2.5	0.5	0.5	Neutron emission time measurement
n ToF-LAND (large neutron detector)	40	5	6	Low yield measurement
n ToF-6 (6 m detector)	5	0.5	6	Ion temperature for DD experiments
n ToF-17 (17 m detector)	5	0.5	17	Ion temperature for DT experiments

$$N_{\gamma,\infty} = Y_n \frac{m}{r^2} k, \tag{3}$$

where k includes the various nuclear quantities, detector efficiencies, and self-absorption factors.

This method is limited, since the calibration requires a source that can produce neutron fluences similar to that expected in experiments. Since the self-absorption and neutron transport in the sample are dependent on the size and shape of the sample, reductions in sample size for high yield targets would result in changes in the efficiency of the system. Maintaining the same sample as used in calibrations will ultimately result in saturation of detection systems. Increasing r or τ_{delay} can, as best, increase the range of the system by a few orders of magnitude.

A second method for calibrating the system[11] utilizes thin foils of activation material in which the contribution of self-absorption and neutron scattering is small. The foil is counted in a geometry that can be reproduced with a traceable gamma-ray calibration source that is used to obtain an absolute calibration for the gamma-ray detector used in analyzing the sample. By utilizing foils and activation reactions with well known nuclear cross sections, isotopic abundances, and branching ratios, Eq. (1) can be used to obtain accurate neutron yields over a wide dynamic range by choosing appropriate reactions and varying the mass of the sample. If η_{sa} and η_{trans} are kept small, their uncertainty can be reduced so as to not contribute significantly to the yield determination. Furthermore, several foils of different elements can be used simultaneously, giving further confidence of the yield determination. Since this method utilizes small samples to keep self-absorption low, it is restricted to higher yields than the previously described system.

It is anticipated that a range of neutron yield will exist for which both systems are useful. Since the two calibrations will be independent, the comparison of results will also increase confidence in the measurement.

B. Current-mode detectors

Current-mode neutron detectors consist of plastic scintillators coupled to fast photomultiplier tubes (Fig. 2) and utilize high-bandwidth transient digitizers. A light signal is produced in the scintillator when recoil protons lose their energy in the plastic. Such systems have been used to measure the neutron yield,[12] ion temperature,[13–17] and neutron emission time[18] of ICF targets on Nova, Omega, and other large ICF

facilities. These systems are relatively inexpensive, have large dynamic range, and have fast time response, making them ideal candidates for a reliable base system of diagnostics.

The NIF current-mode detector system[19] will consist of four detectors (Table II) at three different locations in the NIF target bay. The system will be used to extend the range of yield measurements below that available with the nuclear activation system. It will be used to obtain ion temperatures from the width of the neutron energy spectrum for both DD and DT targets. With the addition of an optical fiducial, a detector located close to the target will be used to obtain neutron emission time.

C. Neutron spectrometer

The Los Alamos National Laboratory (LANL) Tion (pronounced ''tee-ion'') neutron scintillator array[20] will be upgraded[21] and installed for use on the NIF. The array consists of 1020 detectors each made up of a scintillator and photomultiplier tube. The signals are recorded with time-to-digital converters so that a histogram of neutron arrival times can be produced. This system allows the energy distribution of neutrons to be determined.

The array can operate over a yield range from 2×10^7 to 3×10^9 DD neutrons or 6×10^7 to 1×10^{10} DT neutrons. If the primary neutron yield is within this range, the instrument can be used to give the ion temperature,[22] which is how it was used at Nova. However, the higher anticipated yields on the NIF will allow other uses as well.

The DD reaction has two nearly equal branches:

$$D+D \rightarrow p+T, \tag{4}$$

$$D+D \rightarrow n+{}^3\text{He}. \tag{5}$$

The triton (T) produced in the first branch is born with 1.0 MeV, and has a finite chance of reacting with a fuel deuteron to produce a secondary neutron.[23] If the ρR of the fuel is sufficiently low, the triton does not slow significantly on the way out of the fuel, and the probability of reacting is simply proportional to ρR, so that the ratio of secondary to primary neutrons becomes a ρR diagnostic.[24] If, however, the capsule has high ρR, then the triton can slow to thermal energies. In this case, the faster the slowing rate, the fewer the secondary neutrons produced. Since slowing is a strong function of electron temperature, secondary yield then becomes an indicator of electron temperature.
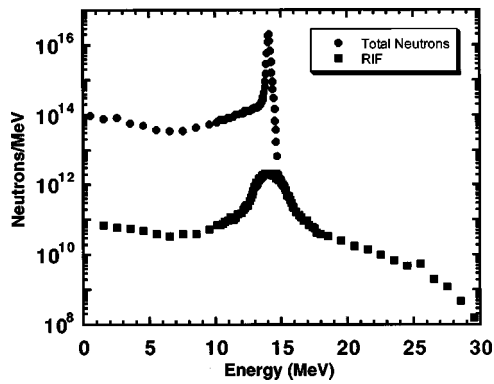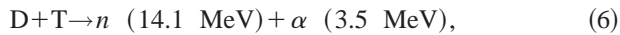
FIG. 3. Calculated tertiary [reaction-in-flight (RIF)] neutrons from a high-convergence NIF capsule as well as the total neutron spectrum.

For high-ρR implosions, tertiary processes[23] come into play:

$$D+T \rightarrow n \ (14.1 \text{ MeV}) + \alpha \ (3.5 \text{ MeV}), \tag{6}$$

$$n+D \rightarrow n' + D' \ (0-12.5 \text{ MeV}), \tag{7}$$

$$D'+T \rightarrow n \ (\text{up to } 30.5 \text{ MeV}) + \alpha, \tag{8}$$

that is, a DT neutron collides with a fuel ion, accelerating it up to many MeV. That fuel ion then has a finite probability of reacting with other fuel ions to produce a very high-energy tertiary neutron. Since this process involves three reactions, the ratio of tertiary to primary neutrons is proportional to $(\rho R)^2$.

The tertiary process leads to a continuum of neutron energies up to the maximum of 30.5 MeV (Fig. 3). The neutron spectrometer will be able to measure the leading edge (in time) of the energy distribution but will saturate before the arrival of the primary neutrons.

Single-hit neutron arrays have been used to characterize mix in ICF implosions either by measuring the yield from deuterated plastic capsule implosions[25] or by measuring the energy spectra of secondary neutrons produced in moderate convergence implosions.[26]

In addition, less sensitive neutron spectrometer arrays consisting of up to 10^4 detectors have been considered.[27] While these may allow more detailed neutron energy spectra to be obtained, techniques for reducing the cost per channel will need to be developed to make such a system practical.

D. Debris and radiochemistry collector

Debris from high-energy-density experiments is of interest, and the core set of the NIF diagnostics will include a debris collector.[28] Nuclear diagnostic personnel are working to ensure that this system can also be utilized for radiochemistry diagnosis of ICF implosions.

Radiochemistry can be used in ICF to infer conditions in the ablator at the time of peak burn. Activation of ablator material or radiochemical tracers by fusion neutrons (and to some extent by charged particles) can take place in an amount that depends on the yield and the ablator areal density ($\rho \Delta R$) at implosion time.

In addition to the debris collector, other techniques, such as collection of activated gases on a cryogenic finger,[29] are being considered.

III. ADVANCED NUCLEAR DIAGNOSTICS

With the higher neutron yields anticipated to be available on the NIF, a number of diagnostic techniques will become available that have, in the past, either not been attempted or have suffered from too little signal. Many of these techniques are currently under development either for the NIF or for other facilities, such as the Omega Laser Facility,[30] where cryogenic direct-drive ICF experiments are scheduled to begin soon.

A. Fusion gamma-ray-based burn history

Burn histories have been measured in ICF experiments using scintillators placed very close to the target.[31] Thin plastic scintillators coupled to streak cameras allow good time resolution, limited by the transit time of neutrons across the thickness of the scintillator.

On the NIF, due to the presence of high-x-ray fluxes from targets and unconverted laser light near the target chamber center, diagnostics will need to remain at a much larger distance from the target chamber center, perhaps as far as 50 cm, to prevent excessive amounts of ablated diagnostic material from being deposited onto the NIF optics.

Since the duration of the burn of an ICF capsule is on the order of 100 ps, time resolution of about 10 ps is required for the measurement. For a 1 keV DT target, the time-of-flight spreading will exceed 10 ps for a detector greater than 8 cm from the target. For higher temperatures or for DD, the distance is even smaller. This prevents the use of neutrons for measuring burn history.

Efforts are underway to utilize the 16.7 MeV gamma-ray-producing branch of the DT reaction for burn history measurements,

$$D+T \rightarrow \gamma + {}^5\text{He}, \tag{9}$$

since photons show no time-of-flight spread. The branching ratio[32] for this reaction is only about 5×10^{-5}, so detecting this reaction on a background of gamma rays produced when the DT neutrons interact with the target, target positioner, and other materials near the target can be difficult.

A number of different techniques have been investigated.[33] Some of the more promising utilize the detection of Cerenkov radiation from relativistic electron–positron pairs created when the gamma ray interacts in a converter of some type. When a charged particle travels in a medium at a speed exceeding the speed of light in that medium, radiation is emitted, primarily in the direction of the motion. This radiation is prompt, and therefore can be used for high bandwidth measurements.

The detection of Cerenkov radiation from an ICF target was attempted using a lead glass detector on Nova.[34] Because of the high lead content and index of refraction, the lead glass served as both a converter and Cerenkov detector. No gammas were detected, but the instrument was found to be sensitive to neutrons interacting in the glass.
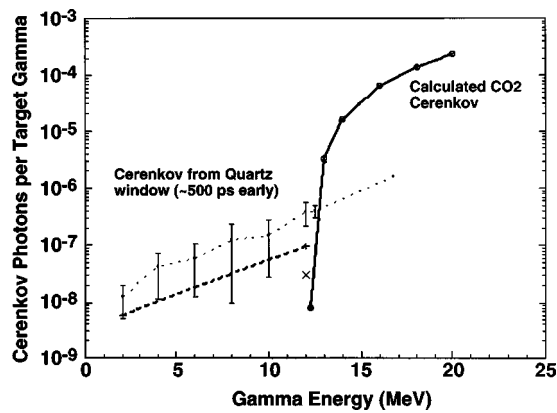
FIG. 4. Detection efficiency of the gas Cerenkov detector. The threshold can be adjusted by changing the gas pressure.

A detector which used a specially shaped acrylic Cerenkov detector and separate converter was more successful. A 1 mm Pb converter and 1 cm Be converter used in the instrument were able to obtain signals at the correct time for gamma rays.[33] Without the converters, the signal was much reduced.

Because of the high index of refraction of this Cerenkov detector, it is sensitive not only to the very high-energy gammas from the DT fusion reaction, but also to much lower energy gammas from reactions of neutrons with materials in or near the target. For experiments in which large amounts of material are near the target, such as a hohlraum or a cryogenic shroud, this contribution could compromise the time response of the signal.

A gas Cerenkov detector[35] allows the threshold of Cerenkov light production to be adjusted by changing the gas pressure in the detector (Fig. 4). Because a gas will typically have an index of refraction that is very close to unity, the gamma detection threshold can be set very high. A system has been designed and fabricated (Fig. 5) for testing on the Omega Laser Facility. This system uses a beryllium converter to produce relativistic electron–positron pairs which emit Cerenkov light while traveling through 2 atm of CO_2 gas. An optical system was designed to collect the light and relay it to a microchannel plate photomultiplier tube for detection. The system has been successfully tested using a linear accelerator both to deliver energetic electrons directly to the detector as well as brehmsstrahlung radiation. The detector will soon be tested using high-yield DT implosions. Following successful detection of fusion gamma rays, the system will be modified to utilize an optical streak camera to
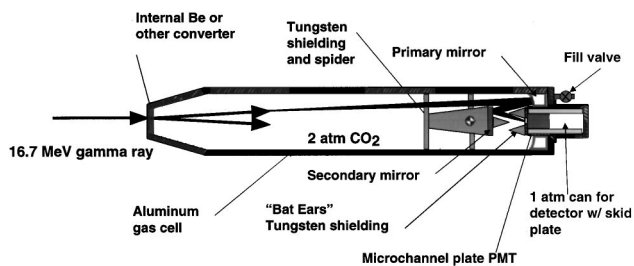

FIG. 5. Design for a gas Cerenkov detector that has been designed and fabricated for use on the Omega Laser Facility.
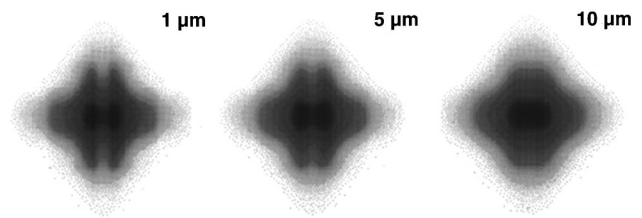

FIG. 6. Simulated neutron images from a NIF capsule that failed due to too large a flux asymmetry driving the capsule. At 10 μm resolution, the asymmetry of the implosion is seen, but details require higher spatial resolution.

provide high-bandwidth burn histories as a demonstration of the utility for the NIF.

B. Neutron imaging

Neutron imaging is currently being investigated computationally to determine its utility for determining failure modes of NIF ignition capsules. From these calculations, the required spatial resolution for an imaging system will be determined. Currently, a resolution of about 10 μm appears to be useful for some purposes, but a resolution of 5 μm may be necessary to see details in the implosion structure (Fig. 6).

In penumbral imaging, an aperture that is larger than the size of the source to be imaged is used. In the detector plane, the detected image consists of an umbra, which is the region which is exposed to the entire source through the aperture, surrounded by the penumbra, the region which is progressively obscured from the source by the aperture edges. The source image is encoded in this measurement and must be decoded.

Neutron imaging has been performed[36] using penumbral apertures[37] and has attained neutron resolution of approximately 60 μm.[38] Apertures have been designed to give a theoretical resolution of 10 μm.[39]

Los Alamos National Laboratory and the Commissariat à l'Energie Atomique (CEA) in France have recently begun a cooperative effort to develop neutron imaging for use on the NIF and the Laser MegaJoule (LMJ).[40] Near term goals will be to determine the potential of each technique to achieve high resolution imaging reliably for the NIF and LMJ, to determine the effectiveness of unfold methods for analyzing penumbral images, and to compare the results from neutron penumbral imaging with that from neutron pinhole imaging. LANL will pursue pinhole imaging[41] and CEA will pursue penumbral imaging.[42]

Neutron imaging requires effort in three areas: pinhole/aperture fabrication, mechanical alignment of the aperture to the target, and development of detectors. Neutron apertures and pinholes, due to the penetrating nature of neutrons, must be very thick (Fig. 7). Since the apertures are narrow, this gives a narrow field of view and alignment tolerances are tight.

C. Charged particle techniques

In addition to neutrons and gamma rays, fusion reactions can produce charged particles which also convey information about the implosion. In some cases, such as the 15 MeV proton produced in the D–^{3}He reaction, these particles can

(a)

30 μm central diameter   0.08° taper angle

2.5 cm

15 cm

(b)

580 μm

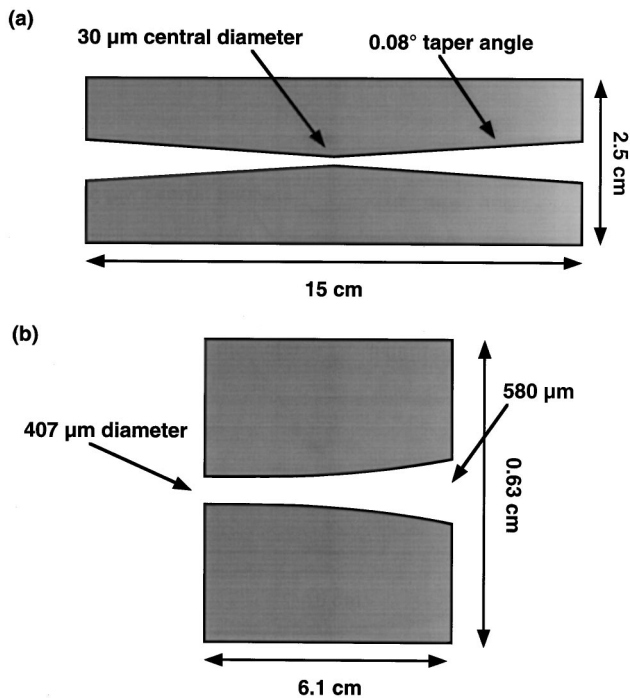407 μm diameter

0.63 cm

6.1 cm

FIG. 7. Comparison of (a) a neutron pinhole that will be fielded on Omega high-yield implosion experiments and (b) a penumbral aperture used on Nova experiments.

be very penetrating and escape the imploded core of a capsule. The availability of charged particle diagnostics allows the measurement of yield from neutronless reactions such as the D–^{3}He reaction,[43] allows measurement of charged particle slowing as the particle traverses the ablator,[43,44] and enables a measurement of fuel ρR from knock-on ions created when fusion neutrons collide with and transfer energy to these ions.[45]

Secondary and tertiary charged particles can also be formed in reaction paths similar to those forming neutrons.[23] The use of these particles for symmetry and ρR measurements has been investigated for the NIF.[46]

D. Recoil proton/deuteron techniques

As was stated earlier, when ion temperatures are measured using neutron time-of-flight spreading, one takes ad-

Magnetic Field
⊗

Array of single-hit detectors

Recoil protons

Current-Mode Detectors

TDCs, ADCs

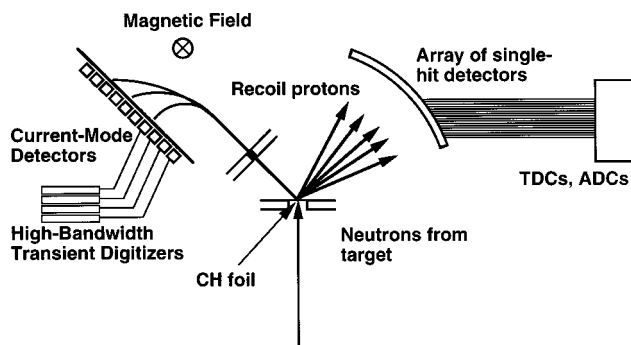High-Bandwidth Transient Digitizers

Neutrons from target

CH foil

FIG. 8. Methods of measuring neutrons using recoil protons using apertured detectors to (left) select a single recoil angle and magnetic field to analyze the proton energy or (right) using detectors that measure the energy of each recoil proton.

vantage of the fact that the neutrons are produced nearly instantaneously and the time spread of their arrival at a detector is taken as due to their energy distribution. When one measures the burn history of a target using a detector close to the target, the nearly monoenergetic nature of the neutrons is utilized. If one would like both time and energy resolution, then a detection method must be used which does not require either assumption.

One method of allowing separate measurement of both the energy and arrival time of a neutron at a detector is by means of the recoil proton technique.[47] Neutrons impinging on a thin plastic foil strike some of the protons, transferring some of their energy to the protons. The energy of the proton is given by

$$E_p = \frac{4(m_p/m_n)}{(m_p/m_n+1)^2} E_n \cos^2 \theta, \tag{10}$$

where E_n is the energy of the neutron incident on the foil, θ is the angle between the original velocity of the neutron and that of the recoil proton, and m_p and m_n are the masses of the proton and neutron, respectively. Approximating the neutron and proton masses to be the same, Eq. (10) reduces to $E_p = E_n \cos^2 \theta$.

Proton energy can be measured in ways other than time of flight, such as through magnetic analyzers or through energy deposition in silicon detectors (Fig. 8). If the recoil protons are apertured to a single angle,[48] then the energy of the protons is, by Eq. (10), proportional to the energy of the neutron. The spread of the proton energy is a measure of the energy spread of the neutrons, thus giving ion temperature information. The time history of the different proton energies can then be used to obtain a time-dependent ion temperature.

Similar information can also be obtained by measuring the arrival time at an array of single-hit detectors.[49] With sufficiently high time resolution time-to-digital converters (TDCs), and amplitude-to-digital converters (ADCs), the energy and arrival time of recoil protons can be measured separately. From these, the energy and arrival time of the neutrons at the foil can be determined. If these are sufficiently well measured, then the energy and birth time of individual neutrons can also be determined.

These techniques require the use of very thin plastic foils since thick foils would lead to slowing of the protons as they leave the foil. In thick foils, recoil protons would be born at different thicknesses in the foil and would lose energy dependent on the location in the foil and the recoil angle.

ACKNOWLEDGMENT

[1] J. A. Paisner, J. D. Boyes, S. A. Kumpan, W. H. Lowdermilk, and M. S. Sorem, Laser Focus World **30**, 75 (1994).
[2] J. Lindl, Phys. Plasmas **2**, 3933 (1995).
[3] R. L. Kauffman *et al.*, Phys. Rev. Lett. **73**, 2320 (1994).
[4] B. A. Remington, S. V. Weber, S. W. Haan, J. D. Kilkenny, S. G. Glendinning, R. J. Wallace, W. H. Goldstein, B. G. Wilson, and J. K. Nash, Phys. Fluids B **5**, 2589 (1993).
[5] A. M. Evans, N. J. Freeman, P. Graham, C. J. Horsfield, S. D. Rothman,

B. R. Thomas, and A. J. Tyrrell, Laser Part. Beams **14**, 113 (1996).

[6] J. C. Fernández *et al.*, Phys. Plasmas **4**, 1849 (1997).

[7] NIF Joint Central Diagnostics Team, The Management Plan for the Diagnostics on the National Ignition Facility, March 8, 2000 (unpublished).

[8] C. L. Ruiz and G. W. Cooper, Rev. Sci. Instrum., these proceedings.

[9] C. W. Barnes, T. J. Murphy, and J. A. Oertel, Rev. Sci. Instrum., these proceedings.

[10] C. L. Ruiz, R. J. Leeper, F. A. Schmidlapp, G. Cooper, and D. J. Malbrough, Rev. Sci. Instrum. **63**, 4889 (1992).

[11] C. W. Barnes, Rev. Sci. Instrum. **68**, 520 (1997).

[12] M. D. Cable and M. B. Nelson, Rev. Sci. Instrum. **59**, 1738 (1988).

[13] R. A. Lerche, L. W. Coleman, J. W. Houghton, D. R. Speck, and E. K. Storm, Appl. Phys. Lett. **31**, 645 (1977).

[14] M. A. Russotto and R. L. Kremens, Rev. Sci. Instrum. **61**, 3125 (1990).

[15] B. A. Remington, R. A. Lerche, and M. D. Cable, Rev. Sci. Instrum. **61**, 3128 (1990).

[16] T. J. Murphy, R. A. Lerche, C. Bennett, and G. Howe, Rev. Sci. Instrum. **66**, 930 (1995).

[17] T. J. Murphy, R. E. Chrien, and K. A. Klare, Rev. Sci. Instrum. **68**, 610 (1997).

[18] R. A. Lerche, D. R. Kania, S. M. Lane, G. L. Tietbohl, C. K. Bennett, and G. P. Baltzer, Rev. Sci. Instrum. **59**, 1697 (1988).

[19] T. J. Murphy, J. L. Jimerson, R. R. Berggren, J. R. Faulkner, J. A. Oertel, and P. J. Walsh, Rev. Sci. Instrum., these proceedings.

[20] R. E. Chrien, D. F. Simmons, and D. L. Holmberg, Rev. Sci. Instrum. **63**, 4886 (1992).

[21] R. G. Watt, R. E. Chrien, K. A. Klare, G. L. Morgan, T. J. Murphy, D. C. Wilson, and S. W. Haan, Rev. Sci. Instrum., these proceedings.

[22] R. E. Chrien, K. A. Klare, and T. J. Murphy, Rev. Sci. Instrum. **68**, 607 (1997).

[23] H. Azechi, M. D. Cable, and R. O. Stapf, Laser Part. Beams **9**, 119 (1991).

[24] M. D. Cable, S. P. Hatchett, and M. B. Nelson, Rev. Sci. Instrum. **63**, 4823 (1992).

[25] R. E. Chrien, N. M. Hoffman, J. D. Colvin, C. J. Keane, O. L. Landen, and B. A. Hammel, Phys. Plasmas **5**, 768 (1998).

[26] M. D. Cable *et al.*, Phys. Rev. Lett. **73**, 2316 (1994).

[27] M. D. Cable, S. M. Lane, R. A. Lerche, S. G. Prussin, and R. G. Vieira, Rev. Sci. Instrum. **57**, 1729 (1986).

[28] M. Miller, Rev. Sci. Instrum., these proceedings.

[29] T. C. Sangster (private communication).

[30] T. R. Boehly *et al.*, Opt. Commun. **133**, 495 (1997).

[31] R. A. Lerche, D. W. Phillion, and G. L. Tietbohl, Rev. Sci. Instrum. **66**, 933 (1995).

[32] F. E. Cecil and F. J. Wilkinson III, Phys. Rev. Lett. **53**, 767 (1984).

[33] M. J. Moran and J. Hall, Rev. Sci. Instrum. **68**, 521 (1997).

[34] R. A. Lerche, M. D. Cable, and D. W. Phillion, Rev. Sci. Instrum. **61**, 3187 (1990).

[35] R. R. Berggren, Rev. Sci. Instrum., these proceedings.

[36] D. B. Ress, R. A. Lerche, R. J. Ellis, and K. A. Nugent, Science **241**, 956 (1988).

[37] R. A. Lerche, D. Ress, R. J. Ellis, S. M. Lane, and K. A. Nugent, Laser Part. Beams **9**, 99 (1991).

[38] R. A. Lerche, D. B. Ress, R. J. Ellis, and S. M. Lane, Rev. Sci. Instrum. **70**, 1220 (1999).

[39] D. B. Ress, Rev. Sci. Instrum. **61**, 3184 (1990).

[40] A. Bettinger and M. Decroisette, Fusion Eng. Des. **46**, 457 (1999).

[41] G. Morgan *et al.*, Rev. Sci. Instrum., these proceedings.

[42] O. Delage, Rev. Sci. Instrum., these proceedings.

[43] C. K. Li *et al.*, Phys. Plasmas **7**, 2578 (2000).

[44] Y. Kitagawa *et al.*, Phys. Rev. Lett. **75**, 3130 (1995).

[45] P. B. Radha, S. Skupsky, R. D. Petrasso, and J. M. Soures, Phys. Plasmas **7**, 1531 (2000).

[46] R. D. Petrasso *et al.*, Phys. Rev. Lett. **77**, 2718 (1996).

[47] J. Kallne and H. Enge, Nucl. Instrum. Methods Phys. Res. A **311**, 595 (1992).

[48] R. J. Leeper, C. L. Ruiz, and G. W. Cooper, Conference Record, 22nd IEEE International Conference on Plasma Science, Madison, Wisconsin, 5–8 June 1995 (unpublished), p. 153.

[49] T. J. Murphy, in Ref. 48, p. 152.